IEEE Access
Multidisciplinary | Rapid Review | Open Access Journal

Received December 31, 2020, accepted January 18, 2021, date of publication February 19, 2021, date of current version March 5, 2021.

Digital Object Identifier 10.1109/ACCESS.2021.3060467

A New Chipless RFID Permittivity Sensor System

YANG WANG[1,2], CHUN-HE QUAN[1], FU-XING LIU[1], XIAO-YU ZHANG[1], AND JONG-CHUL LEE[1], (Senior Member, IEEE)

[1]Department of Radio Science and Engineering, Kwangwoon University, Seoul 139-701, South Korea
[2]Beijing Metamaterials Information Technology Company Ltd., Beijing 102600, China

Corresponding author: Jong-Chul Lee (jclee@kw.ac.kr)

This work was supported in part by the Research Grant of Kwangwoon University 2019, and in part by the BK21 Four project (Wellness Care Fusion Technology Based on Hyper-Connected Human Experiences) funded by the Ministry of Education, South Korea, under Grant F20YY8101058.

ABSTRACT Permittivity sensing is commonly utilized in multiple fields for various applications. In this study, an enhanced RFID (Radio Frequency Identification) permittivity sensor system is designed. Additionally, we investigated the signal processing procedures in a stepwise manner to obtain the resultant graphs. For validation, a simplified system including a reader and a tag is tested. The reader in the system comprises a pulse generator and a pair of antennas connected to an oscilloscope, whereas the tag comprises an antenna and a delay line sensor. The pulse generator produces short pulses of less than 1 *ns* periodically, whereas the short-ended delay line on the tag acts as a sensor, wherein the delay time of the traversing wave is primarily associated with the relative permittivity of the material under test (MUT). We tested the system to derive an equation for the value of relative permittivity of the MUT using the measured signal. The system was calibrated by performing both unloaded and air tests to obtain measurement equations. Moreover, an additional test validated the water permittivity sensing, and the relative permittivity measured was 78.1. Considering the errors affecting the measurements, the measured relative permittivity of water concurs with the actual value.

INDEX TERMS Chipless, delay line, permittivity, RFID, sensors.

I. INTRODUCTION

Sensors are commonly used to measure different properties of a material. Among the multiple types of sensing techniques, permittivity sensing is applied in various fields, including biomedicine, agriculture, architecture, and automobile manufacturing [1]–[4].

Several methods, such as the transmission line method, resonant technique, open-ended coaxial probe method, time-domain reflectometry (TDR), and free-space method, are used to test the permittivity [5]–[8]. In applications such as safety and engine monitoring system, portable measuring devices that can collect information in real-time are highly preferred. Generally, the laboratory equipment (e.g., testing probes) required to monitor the materials are extremely bulky and warrant high implementation cost. Therefore, several studies suggested wireless testing and reported structural health monitoring applications using radio frequency identification (RFID) sensors [9]–[12]. In the case of RFID sensors, the reflection spectrum can carry substantial information including permittivity. However, the limited detecting range must be designed specifically based on the requirements. For instance, a remote testing technique was designed for corrosion characterization based on frequency selective surface design and feature fusion to generate resonances and enhance the sensitivity and reliability of the system [13].

This study investigated the feasibility of a chipless RFID permittivity sensor. The operating frequency of the sensor was set to 2.45 *GHz*, which lies within the industrial, scientific, and medical (ISM) frequency band. We applied and tested the remote monitoring technique for ease of control in water, verifying the ability of the proposed system to be applied in various environments.

II. THEORY

The proposed system is implemented based on RFID technology using a transmitter, tag, and receiver/monitor. The tag is attached to or dipped in the material under test (MUT) depending on the type of material. Additionally, the tag includes a sensor that translates the permittivity of the MUT into an electrical signal. The receiver recognizes this signal and displays the result on a monitor. Fig. 1 depicts the system

The associate editor coordinating the review of this manuscript and approving it for publication was Weiren Zhu.

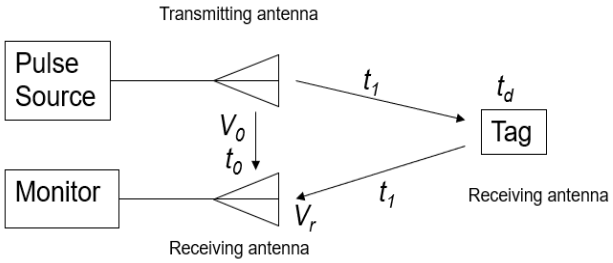

FIGURE 1. System block of the RFID permittivity sensor.

block of the RFID permittivity sensor. For simplification, no amplifiers are included in the tested system.

A. SYSTEM OVERVIEW

As illustrated in Fig. 1, the pulse generated from the source passes through the antenna before being transmitted through the air. The transmitting antenna is a microstrip antenna with a filtering characteristic at 2.45 GHz. The receiving antenna awaits the response signal that consists of two parts. The first part of the signal is directly coupled from the transmitter (V_0), whereas the second part is reflected from the tag (V_r). As the receiving and transmitting antennas are adjacent to each other, the transmission time t_0 between the two antennas is considered to be 0. A 6-GHz oscilloscope with a sampling rate of 20 GSa/s acts as a reader to display the waveform of $V_0 + V_r$. The delay time between V_0 and V_r measured by the oscilloscope in the reading range indicates the total travel time of V_r, calculated using (1).

$$t_{measure} = 2t_1 + t_d \tag{1}$$

where t_1 and t_d denote the time spent by the signal traveling in air and the time delay generated in the tag, respectively. The sensor implemented in the tag generates t_d, and the permittivity of the MUT affects the group delay of the wave in the sensor. Therefore, the measured t_d is directly associated with the MUT permittivity.

B. DESIGN OF THE TAG

The tag constitutes the key component in the system, comprising a permittivity sensor and a broadband monopole patch antenna to maintain a stable received signal.

The permittivity sensor is the core of the proposed RFID system, as the reading cycle of the sensor affected by the MUT permittivity is converted into an electrical characteristic, which in this case is the time delay. Fig. 2 illustrates the schematic of the delay line sensor based on the type of delay line selected for the experiment. Typically, the delay line must be long enough.

The sensor uses a pulse wave rather than a continuous wave. The pulse wave generated at the input port of the sensor in the tag antenna travels through the delay line within a certain time. Subsequently, the reflector directs this wave to the input of the delay line. The delay line can be open-ended, short-ended, or terminated by a capacitive load, wherein each

FIGURE 2. Schematic of the delay line sensor.

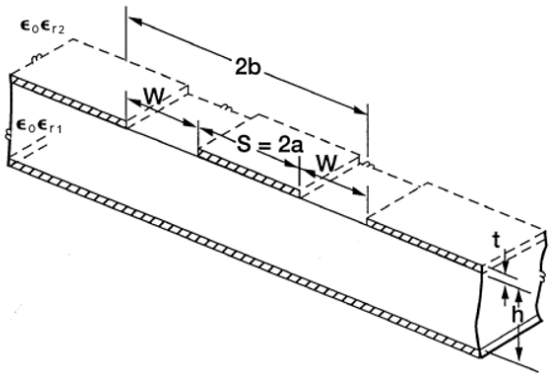

FIGURE 3. Schematic of the grounded coplanar waveguide (GCPW) [15].

of these types differs in terms of phase. We used the short-ended reflector in our experiment owing to its optimal performance with minimal noise. The pulse reflected from the end of the delay line travels into the antenna as a reflected signal. Further investigations are needed to calculate the total time spent by the pulse in the delay line.

The structure of the delay line is selected considering that the field generated on the transmission line can penetrate the MUT, which affects the transmission line characteristics [14]. Moreover, the loss should be sufficiently small for a long transmission line. Thus, the grounded coplanar waveguide (GCPW) is suitable for the delay line application [15].

The effective permittivity ε_{eff} of GCPW is calculated using (2) [15].

$$\varepsilon_{eff} = \frac{\varepsilon_{r2} + \varepsilon_{r1}\varepsilon_{r2}\frac{K(k')}{K(k)}\frac{K(k_3)}{K(k_3')}}{1 + \frac{K(k')}{K(k)}\frac{K(k_3)}{K(k_3')}} \tag{2}$$

where ε_0 denotes the permittivity of air and ε_1 and ε_2 represent the values of relative permittivity of the substrate and metal conductor, respectively. Additionally, $k = a/b$, $k' = \sqrt{1-k^2}$, $k_3 = tanh(\pi a/2h)/tanh(\pi b/2h)$, and $k_3' = \sqrt{1-k_3^2}$. Equation (2) suggests that ε_{eff} is proportional to the ratio of h to b irrespective of the ratio of S and W [15]. This implies that the widths of S and W must be narrow to achieve maximum effective permittivity.

The total time (t_x) required for a pulse to traverse through GCPW in a single direction can be calculated using (3).

$$t_x = \frac{l}{c}\sqrt{\varepsilon_{eff}} \tag{3}$$

where l denotes the physical length of the GCPW and c is the speed of light ($3 \times 10^8\ m/s$). As the pulse travels a round-trip

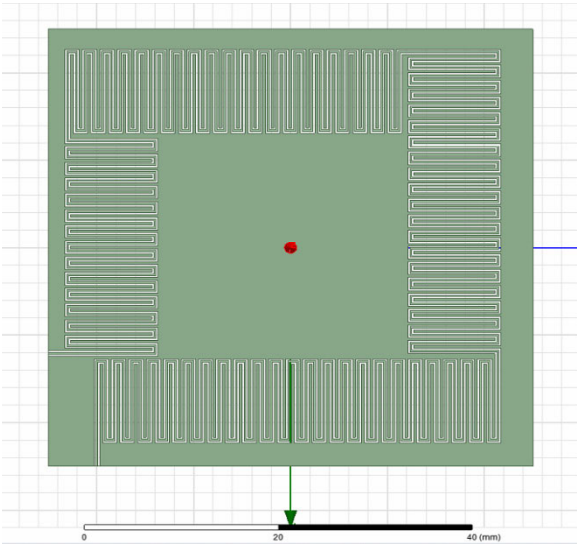

FIGURE 4. Layout of the delay line.

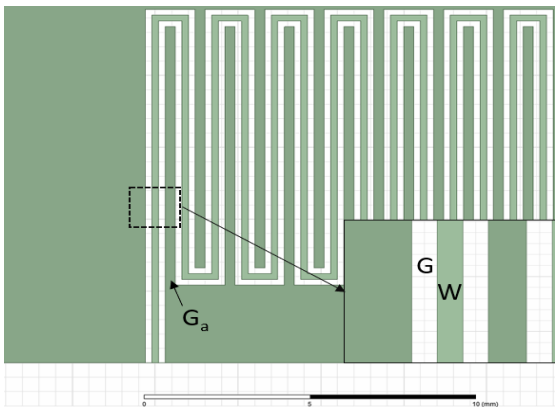

FIGURE 5. Delay line with the size details.

in our design, the time (t_d) required for the signal to enter the delay line and return is determined using (4)

$$t_d = 2t_x = \frac{2l}{c}\sqrt{\varepsilon_{eff}} \tag{4}$$

The delay time is directly associated with the delay line structure and MUT permittivity. The transmission line-type delay line must be sufficiently long in a certain area. Furthermore, we did not consider the characteristic impedance as the designed antenna matches the impedance of the feed line. However, in the case of self-designed printed circuit boards, the transmission line width (W) and gap (G) must be practically feasible. Figs. 4 and 5 depict the design layout and details of the delay line used in this study.

We fabricated the sensor on a Teflon substrate using the etching process. The total area of the sensor is 50 $mm \times 50$ mm with the line width and gap as 0.2 mm for ease of fabrication; a gap (G_a) of 0.3 mm is maintained between two lines. We performed a transient simulation using Ansys HFSS 19.2 to simulate a pulse traveling through the delay line [16]. The ADS

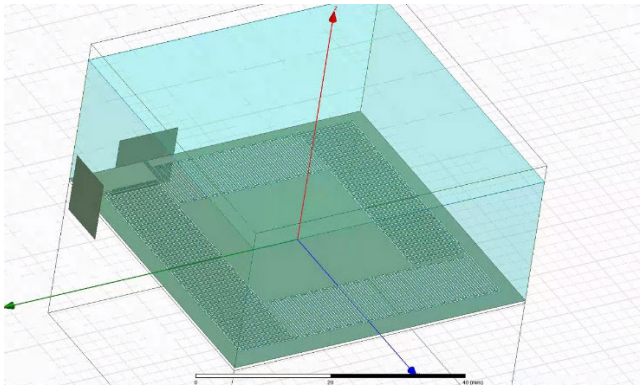

FIGURE 6. Simulated sensor model with a water layer.

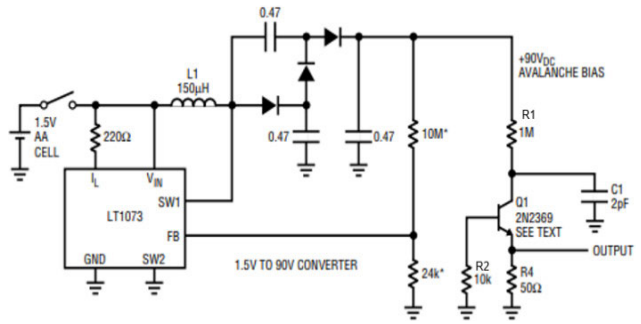

FIGURE 7. Avalanche pulse generator circuit [18].

2016.01 software determined the characteristic impedance as 105 Ω, which concurred with the simulated results. Additionally, the one-way delay time t_{x1} was calculated as 1.41 ns. The light blue region in Fig. 6 indicates the water layer that covered the sensor, in which the permittivity of water is set to 78.9 [17]. The simulated one-way delay t_{x2} was obtained as 12.61 ns.

C. EXPERIMENTAL SYSTEM SETUP

Fig. 7 depicts the avalanche pulse generator circuit adopted from the application note on 2N2369 transistor by Jim Williams [18]. It generates narrow-width pulses of 750 ps from the reader transmitter (Fig. 8). The transmitter antenna is a narrow band microstrip patch antenna operating at 2.45 GHz with a maximum gain of 5 dBi. The patch size is 28 $mm \times 38$ mm, which is associated with the center frequency of the antenna. The feedline width corresponding to a 50-ohm transmission line is 1.5 mm. Furthermore, the receiving antennas are monopole patch antennas with broad bandwidths. The antennas are fabricated using a substrate with dielectric constant, thickness, and loss tangent of 2.54, 0.54 mm, and 0.002, respectively.

Figs. 9 and 10 depict the completed modules used for the experimental analysis.

III. EXPERIMENTS

The relationship between the permittivity of MUT and t_d can be derived using (2) to (4).

$$t_d = A\sqrt{\varepsilon_{MUT}} \tag{5}$$

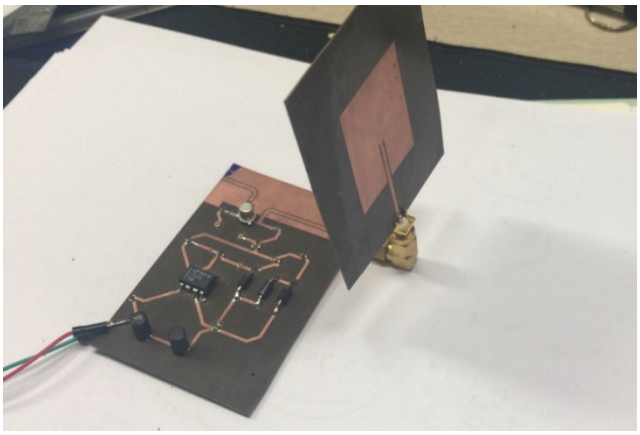

FIGURE 8. The reader transmitter.

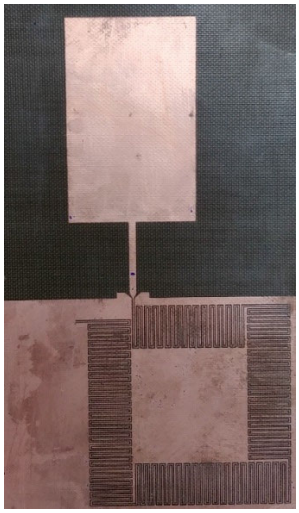

FIGURE 9. The tag of the RFID permittivity sensor.

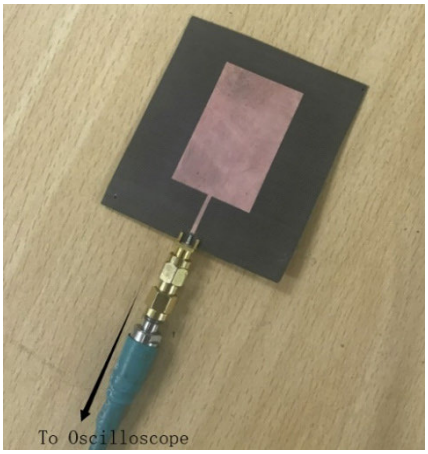

FIGURE 10. The reader receiver.

where ε_{MUT}, which is the main factor affecting the propagation time along the direction of delay line, denotes the relative permittivity of the substrate MUT, and A is a constant associated with the delay line structure to be derived experimentally. As (5) represents a simple proportional function between t_d and $\sqrt{\varepsilon_{MUT}}$, a single test is sufficient to obtain the coefficient of A. Additionally, the actual distance between the tag and reader must be measured to determine the results accurately.

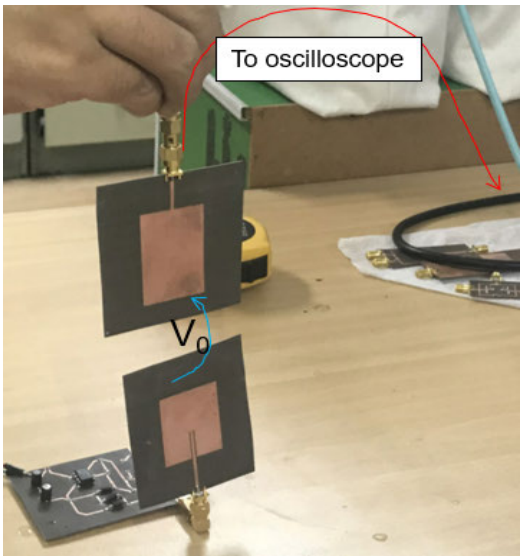

FIGURE 11. The unloaded test.

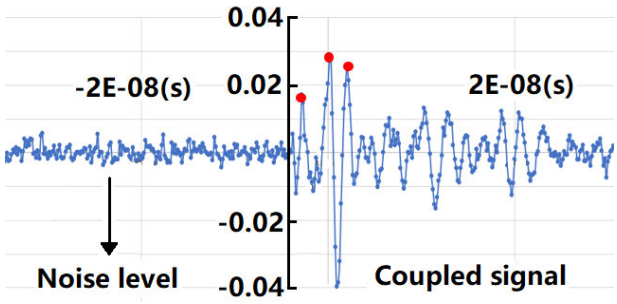

FIGURE 12. Unloaded coupled signal.

A. REFERENCE SIGNAL MEASUREMENT

Fig. 11 depicts the unloaded test setup, wherein the transmitter antenna is placed directly below the receiver antenna without any tag. The reference signal V_0 (Fig. 1) is detected using this test, and the captured signal is illustrated in Fig. 12 with the x-axis and y-axis indicating the time and amplitude, respectively. Initially, the noise level is observed before the generation of the signal waveform. We recorded the first three peaks of the measured waveform and considered them as reference for the remaining tests.

B. AIR TEST AND EQUATION DERIVATION

Fig. 13 depicts the air test setup, wherein the tag is placed along with the transmitter and receiver antennas. A test was performed to capture the received signal $(V_r + V_0)$ in the air. V_0 indicates the same signal observed in the unloaded test and

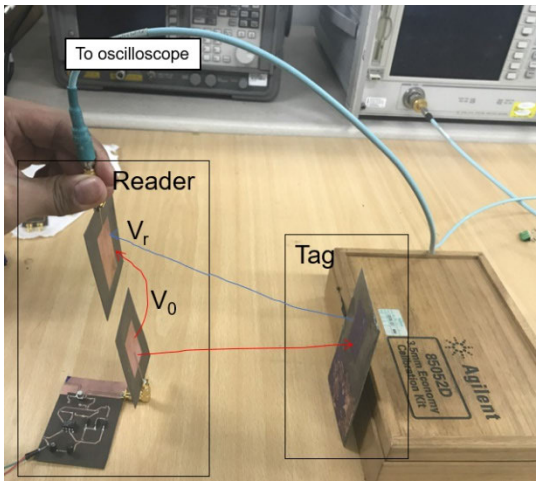

FIGURE 13. The test setup in the air.

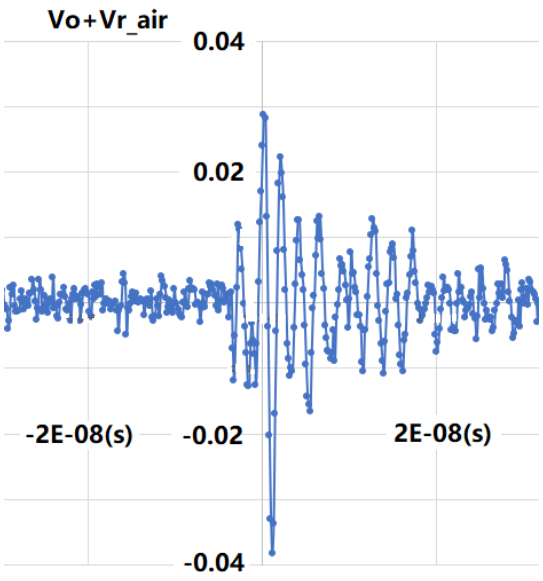

FIGURE 14. The test setup in the air.

V_r is the reflected signal from the tag. Fig. 14 illustrates the received signal observed by the oscilloscope.

The waveform in Fig. 14 does not differ significantly from that observed in Fig. 12. This is because V_r is close to V_0 and the two components nearly overlap with each other. The V_0 component in the air test is identical to that of V_0 obtained from the unloaded test without the tag. To obtain restored V_r, we subtracted the waveform of V_0 in Fig. 12 from that of Fig. 14. As indicated in Fig. 15, the shapes of the first three peaks and first valley of the restored V_r are identical to those of V_0. Equation (1) calculates the time delay between the restored V_r and V_0, denoted by $t_{measure}$.

The value of $t_{measure}$ was found to be 3.818 ns. Owing to the use of RFID technology in signal transmission, the distance s between the reader and tag is limited, the value of s was calculated to be 0.15 m. Furthermore, the travelling time of

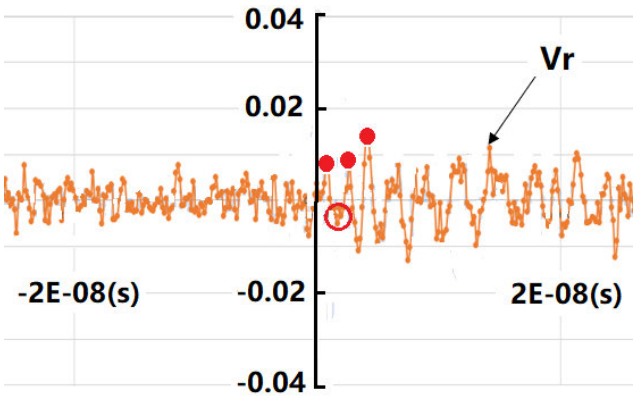

FIGURE 15. The resorted V_r signal.

the signal in air can be determined using (6).

$$2t_1 = \frac{2s}{c} \tag{6}$$

Considering the time spent in the RFID tag, the delay time is obtained using $t_d = t_{measure} - 2t_1 = 2.818\,ns$. As the relative permittivity of air is $\varepsilon_{air} = 1$, the value of A in (5) is obtained as 2.818. Thus, the relationship between the delay time in the tag and the MUT relative permittivity is obtained using (7).

$$t_d = 2.818\sqrt{\varepsilon_{MUT}} \times 10^{-9} \tag{7}$$

where the unit of t_d is seconds. Equation (7) is the final derived relationship used in the subsequent validation test.

C. VALIDATION TEST WITH WATER

We tested the permittivity of water at 25 $^\circ C$ using the derived relationship in (7). Fig. 16 depicts the experimental setup in water, wherein substantial loss is observed in the water environment owing to the tag being dipped in water. The thickness of the container is sufficiently thin to be ignored. The experiment was conducted identical to the air test. The result obtained is depicted in Fig. 17.

Based on the simulation results, a time delay of few seconds is expected. As the two components in the received waveform do not overlap, a subtraction is not required. The three vertical lines in Fig. 17 indicate the three small peaks where V_0 exhibits the noise. The pattern of these three peaks with an oscillation after the first peak is identical to the one observed in Fig. 14. This pattern indicates the waveform reflected by the tag (V_r) as it cannot originate elsewhere. The time delay $t_{measure}$ between V_0 and V_r is 31.12 ns. Thus, the relationship derived in (4) and (5) is used to calculate the permittivity of water.

In (1), t_1 denotes the time required for the signal to travel through the path between the reader and tag. The distance s of the path is 0.15 m, comprising the distance values of water $S_w = 0.1\ m$ and air $S_a = 0.05\ m$, with the water relative permittivity of ε_{rw}. Therefore, the delay time is measured

FIGURE 16. Test setup with water.

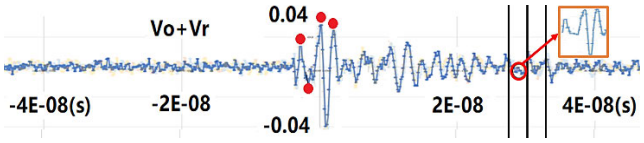

FIGURE 17. Result of the water test.

using (8).

$$t_{measure} = 2t_1 + t_d = 2\left(\frac{S_a}{c} + \frac{S_w}{c}\sqrt{\varepsilon_{rw}}\right) + t_d$$
$$= \frac{2S_a}{c} + \sqrt{\varepsilon_{rw}}\left(\frac{2S_w}{c} + 2.818 \times 10^{-9}\right) \quad (8)$$

The relative permittivity of water is determined as $\varepsilon_{rw} = 78.1$, considering $t_{measure} = 31.12\ ns$.

The air and water are applied as the actual operating environment in this measurement, and the error exists primarily in the measurement of the distance between the reader and tag.

IV. CONCLUSION

We designed a simplified chipless RFID permittivity sensor system comprising a reader and tag. The system was tested in air and water environments, and the corresponding signal processing procedures were determined in a stepwise manner. Furthermore, the experimental test was performed for individual components considering detailed circuit structures. We derived an equation to convert the measured signal into the relative permittivity value of the MUT. The system was calibrated to obtain a reference signal based on an unloaded test, and the measurement equations were determined through an air test. Subsequently, we conducted a validation test to obtain the value of water permittivity sensing. The water test was used to simulate the environment where the proposed system can be potentially applied, and the equations derived from the test were validated. The measured relative permittivity of water was 78.1. Considering the errors induced in the measurement, the result agreed with the actual value of relative permittivity of water. Thus, the proposed permittivity sensor system can be used to measure the permittivity of other materials.

This sensor can be applied in various environments or machines to test the permittivity of the liquid and evaluate the water quality. In the future, we intend to design a more compact structure to access unreachable target materials. Additionally, further investigations are necessary to obtain measurement methods with enhanced precision, better waterproof performance, higher working frequency, and advanced processing technology.

REFERENCES

[1] O. Sipahioglu and S. A. Barringer, "Dielectric properties of vegetables and fruits as a function of temperature, ash, and moisture content," *J. Food Sci.*, vol. 68, no. 1, pp. 234–239, Jan. 2003.
[2] W. J. Fleming, "New automotive sensors—A review," *IEEE Sensors J.*, vol. 8, no. 11, pp. 1900–1921, Nov. 2008.
[3] G. de Graaf, G. Lacerenza, R. Wolffenbuttel, and J. Visser, "Dielectric spectroscopy for measuring the composition of gasoline/water/ethanol mixtures," in *Proc. IEEE Int. Instrum. Meas. Technol. Conf. (I MTC)*, May 2015, pp. 154–158.
[4] E. Topsakal, T. Karacolak, and E. C. Moreland, "Glucose-dependent dielectric properties of blood plasma," in *Proc. 30th URSI Gen. Assem. Sci. Symp.*, Aug. 2011, pp. 1–4.
[5] I. Piekarz, J. Sorocki, K. Wincza, and S. Gruszczynski, "Liquids permittivity measurement using two-wire transmission line sensor," *IEEE Sensors J.*, vol. 18, no. 18, pp. 7458–7466, Jul. 2018.
[6] O. Siddiqui, R. Ramzan, M. Amin, and O. M. Ramahi, "A non-invasive phase sensor for permittivity and moisture estimation based on anomalous dispersion," *Sci. Rep.*, vol. 6, no. 1, pp. 1–9, Jun. 2016.
[7] X. Zhang, C. Ruan, T. Haq, and K. Chen, "High-sensitivity microwave sensor for liquid characterization using a complementary circular spiral resonator," *Sensors*, vol. 19, no. 4, p. 787, Feb. 2019.
[8] M. S. Venkatesh and G. S. V. Raghavan, "An overview of dielectric properties measuring techniques," *Can. Biosyst. Eng.*, vol. 47, no. 4, pp. 15–30, Jan. 2005.
[9] H. Lobato-Morales, A. Corona-Chávez, J. L. Olvera-Cervantes, R. A. Chávez-Pérez, and J. L. Medina-Monroy, "Wireless sensing of complex dielectric permittivity of liquids based on the RFID," *IEEE Trans. Microw. Theory Techn.*, vol. 62, no. 9, pp. 2160–2167, Sep. 2014.
[10] J. Virtanen, L. Ukkonen, T. Björninen, and L. Sydänheimo, "Printed humidity sensor for UHF RFID systems," in *Proc. IEEE Sensors Appl. Symp. (SAS)*, Feb. 2010, pp. 269–272.
[11] A. Lázaro, R. Villarino, F. Costa, S. Genovesi, A. Gentile, L. Buoncristiani, and D. Girbau, "Chipless dielectric constant sensor for structural health testing," *IEEE Sensors J.*, vol. 18, no. 13, pp. 5576–5585, Jul. 2018.
[12] J. Zhang, G. Y. Tian, A. M. J. Marindra, A. I. Sunny, and A. B. Zhao, "A review of passive RFID tag antenna-based sensors and systems for structural health monitoring applications," *Sensors*, vol. 17, no. 2, pp. 1–33, Jan. 2017.
[13] A. M. J. Marindra and G. Y. Tian, "Chipless RFID sensor for corrosion characterization based on frequency selective surface and feature fusion," *Smart Mater. Struct.*, vol. 29, no. 12, Oct. 2020, Art. no. 125010.
[14] Y. Wang and J.-C. Lee, "A miniaturized Marchand balun model with short-end and capacitive feeding," *IEEE Access*, vol. 6, pp. 26653–26659, 2018.
[15] N. S. Rainee, *Coplanar Waveguide Circuits, Components, and Systems*, vol. 165. Hoboken, NJ, USA: Wiley, 2004.
[16] H.-X. Xu, G.-M. Wang, M.-Q. Qi, C.-X. Zhang, J.-G. Liang, J.-Q. Gong, and Y.-C. Zhou, "Analysis and design of two-dimensional resonant-type composite right/left-handed transmission lines with compact gain-enhanced resonant antennas," *IEEE Trans. Antennas Propag.*, vol. 61, no. 2, pp. 735–747, Feb. 2013.
[17] T. Sato, A. Chiba, and R. Nozaki, "Dynamical aspects of mixing schemes in ethanol–water mixtures in terms of the excess partial molar activation free energy, enthalpy, and entropy of the dielectric relaxation process," *J. Chem. Phys.*, vol. 110, no. 5, pp. 2508–2521, Feb. 1999.
[18] J. Williams. *High Speed Amplifier Techniques: A Designer's Companion for Wideband Circuitry*. [Online]. Available: https://www.analog.com/media/en/technical-documentation/application-notes/an47fa.pdf

YANG WANG received the B.S. degree in electronics and information engineering from the Harbin Institute of Technology (HIT), China, in 2013, and the Ph.D. degree from the WICS Laboratory, Kwangwoon University, South Korea, under the supervision of Prof. Jong-Chul Lee.

Since 2013, he has been with the WICS Laboratory, Kwangwoon University. He is currently a Research Engineer with Beijing Metamaterials Information Technology Company Ltd. His research interests include RF design and electromagnetic metamaterials.

CHUN-HE QUAN received the B.S. degree in electronics and information engineering from the Harbin Institute of Technology (HIT), China, in 2013. He is currently pursuing the Ph.D. degree with the WICS Laboratory, Kwangwoon University, South Korea, under the supervision of Prof. Jong-Chul Lee.

Since 2013, he has been with the WICS Laboratory, Kwangwoon University. His research interests include RF design and antenna.

FU-XING LIU received the B.S. degree in integrated circuit design and integration systems from the Qingdao University of Science and Technology (QUST), China, in 2016, and the Ph.D. degree from the WICS Laboratory, Kwangwoon University, South Korea, in 2020, under the supervision of Prof. Jong-Chul Lee. Since 2016, he has been with the WICS Laboratory, Kwangwoon University. He currently participates in a government project named BK21-4 with the Department of Electronics Convergence Engineering, Kwangwoon University. His research interests include RF passive and active devices, electromagnetic metamaterials, and RF sensors.

XIAO-YU ZHANG received the B.S. degree in communication engineering from the Qingdao University of Science and Technology (QUST), China, in 2015. She is currently pursuing the Ph.D. degree with the WICS Laboratory, Kwangwoon University, South Korea, under the supervision of Prof. Jong-Chul Lee.

Since 2015, she has been with the WICS Laboratory, Kwangwoon University. Her research interests include RF design, antenna, and the fifth generation of wireless systems (5G).

JONG-CHUL LEE (Senior Member, IEEE) received the B.S. and M.S. degrees in electronic engineering from Hanyang University, Seoul, South Korea, in 1983 and 1985, respectively, the M.S. degree in electrical engineering from Arizona State University, Tempe, AZ, USA, in December 1989, and the Ph.D. degree in electrical engineering from Texas A&M University, College Station, TX, USA, in May 1994. From June 1994 to February 1996, he was a Senior Researcher with the Photonic Devices Laboratory, the System IC Research and Development Laboratory, and Hyundai Electronics Ind. Company Ltd., South Korea, where he was involved in the development of several high-speed laser diodes and photo diodes, and transmitter/receiver modules. Then, he joined the Department of Radio Science and Engineering with Kwangwoon University, Seoul, where he is currently a Professor. He also served as a Project Director for the ITRC RFIC Center, Kwangwoon University, which was funded by the Ministry of Information and Communication, from August 2000 to August 2007. He has been a Guest Professor with the Department of Electronics and Communication Engineering, Harbin Institute of Technology, since December 2001. He was a Visiting Scholar with the Department of Electrical and Computer Engineering, University of California, San Diego, CA, USA, from December 2002 to February 2004. He is currently participates in several government projects related to the microwave and millimeter wave devices. He has authored and coauthored over 200 papers in international conferences and journals. His research interests include RF MEMS, RF application for ferroelectric materials, microwave and millimeter-wave passive and active devices, electromagnetic metamaterials, IT convergence with bio-medical devices, and energy harvesting devices.